Parasitol Res (2015) 114:659–670
DOI 10.1007/s00436-014-4230-0

ORIGINAL PAPER

Clonorchis sinensis ferritin heavy chain triggers free radicals and mediates inflammation signaling in human hepatic stellate cells

Qiang Mao · Zhizhi Xie · Xiaoyun Wang · Wenjun Chen · Mengyu Ren · Mei Shang · Huali Lei · Yanli Tian · Shan Li · Pei Liang · Tingjin Chen · Chi Liang · Jin Xu · Xuerong Li · Yan Huang · Xinbing Yu

Received: 30 October 2014 / Accepted: 6 November 2014 / Published online: 22 November 2014

Abstract Clonorchiasis, caused by direct and continuous contact with *Clonorchis sinensis*, is associated with hepatobiliary damage, inflammation, periductal fibrosis, and the development of cholangiocarcinoma. Hepatic stellate cells respond to liver injury through production of proinflammatory mediators which drive fibrogenesis; however, their endogenous sources and pathophysiological roles in host cells were not determined. *C. sinensis* ferritin heavy chain (*Cs*FHC) was previously confirmed as a component of excretory/secretory products and exhibited a number of extrahepatic immunomodulatory properties in various diseases. In this study, we investigated the expression pattern and biological role of *Cs*FHC in *C. sinensis*. *Cs*FHC was expressed throughout life stages of *C. sinensis*. More importantly, we found that treatment of human hepatic stellate cell line LX-2 with *Cs*FHC triggered the production of free radicals via time-dependent activation of NADPH oxidase, xanthine oxidase, and inducible nitric oxide synthase. The increase in free radicals substantially promoted the degradation of cytosolic IκBα and nuclear translocation of NF-κB subunits (p65 and p50). *Cs*FHC-induced NF-κB activation was markedly attenuated by preincubation with specific inhibitors of corresponding free radical-producing enzyme or the antioxidant. In addition, *Cs*FHC induced an increased expression level of proinflammatory cytokines, IL-1β and IL-6, in NF-κB-dependent manner. Our results indicate that *Cs*FHC-triggered free radical-mediated NF-κB signaling is an important factor in the chronic inflammation caused by *C. sinensis* infection.

Keywords *Clonorchis sinensis* · Ferritin · Free radicals · Inflammation · HSCs

Introduction

Clonorchiasis is food-borne trematodiasis caused by chronic infection with *Clonorchis sinensis* (*C. sinensis*) (Lv et al. 2012; Wang et al. 2012). *C. sinensis* has afflicted over 35 million people in eastern Asian countries, where clonorchiasis constitutes a significant public health concern. *C. sinensis* reside in the peripheral bile ducts and provoke pathological changes such as inflammation, dilatation, hyperplasia, fibrosis, and cholangiocarcinoma (Chen et al. 2014; Huang et al. 2012; Lim et al. 2008). However, molecular mechanism of clonorchiasis still remains to be elucidated. It was suggested that excretory/secretory products (ESPs) released by liver flukes may lead to pathologic changes in biliary epithelial cells or trigger cellular signals involved in hepatic fibrosis (Kim et al. 2009). ESPs are protein complex including proteases, antioxidant enzymes, and metabolic enzymes. It was reported that human cells exposed to ESPs from liver flukes (*C. sinensis*, *Fasciola hepatica*, and *Opisthorchis viverrini*) displayed diverse pathophysiological responses including proliferation (Lim et al. 2008), apoptosis (Serradell et al. 2007), and inflammation (Pinlaor et al. 2005). Our lab previously

Qiang Mao and Zhizhi Xie contributed equally to this work.

Q. Mao · Z. Xie · X. Wang · W. Chen · M. Ren · M. Shang · H. Lei · Y. Tian · S. Li · P. Liang · T. Chen · C. Liang · J. Xu · X. Li · Y. Huang (✉) · X. Yu (✉)
Department of Parasitology, Zhongshan School of Medicine, Sun Yat-sen University, Guangzhou, Guangdong 510080, China
e-mail: huang66@mail.sysu.edu.cn
e-mail: yuhxteam@163.com

Q. Mao · Z. Xie · X. Wang · W. Chen · M. Ren · M. Shang · H. Lei · Y. Tian · S. Li · P. Liang · T. Chen · C. Liang · J. Xu · X. Li · Y. Huang · X. Yu
Key Laboratory for Tropical Diseases Control of Ministry of Education, Sun Yat-sen University, Guangzhou, Guangdong 510080, China

demonstrated that *C. sinensis* ESPs (*Cs*ESPs) could promote proliferation of human hepatic stellate cell (HSC) line LX-2 (a model cell line in hepatic fibrogenesis) and the effect of *Cs*ESPs was confirmed in animal model (Hu et al. 2009; Ma et al. 2007).

The transcription factor nuclear factor kappa B (NF-κB) has been shown to play a crucial role in HSC survival (Elsharkawy and Mann 2007). In addition, NF-κB has been reported to be upregulated in mouse RAW 264.7 macrophage cells treated with crude extracts from *O. viverrini* and in the nucleus of bile duct epithelial cells of *O. viverrini*-infected hamsters, suggesting the involvement of NF-κB activation in liver fluke infection (Pinlaor et al. 2006). NF-κB is a dimer of Rel family proteins, the most prevalent form of which consists of a heterodimer of RelA (p65) and p50. In the resting state, NF-κB is sequestered in the cytoplasm through covalent binding with inhibitory proteins called IκBs. Exposure of cells to external stimuli, including H_2O_2, ionizing radiation, cytokines, or bacterial endotoxins, results in activation of IκB and its subsequent proteolytic degradation (Morgan and Liu 2011).

Endogenous free radicals, including reactive oxygen species (ROS) and reactive nitrogen species (RNS), are produced through multiple sources including the electron transport chain in mitochondria and as by-products of enzymatic reactions involving NADPH oxidases (NOX), xanthine oxidase (XO), lipoxygenases (LO), cyclooxygenases (COX), and nitric oxide synthases (NOS). Excess intracellular free-radical generation can activate NF-κB and promotes serious cellular injuries and contributes to several human diseases (Morgan and Liu 2011). It was recently reported that treatment of human cholangiocarcinoma cells with *Cs*ESPs triggered increases in free radicals which participate in nuclear factor-κB-mediated inflammation in hepatobiliary diseases (Liang et al. 2013; Nam et al. 2012). However, the key components of *Cs*ESPs that play a major role in *C. sinensis*-induced activation of NF-κB are still under investigation.

In our previous study, using proteomic approaches, we identified the components of *Cs*ESPs, among which *C. sinensis* ferritin heavy chain (*Cs*FHC) was suggested as a key component (Zheng et al. 2011). Ferritin heavy chain is a ferroxidase enzyme responsible for iron storage in prokaryotes and eukaryotes (Theil 1987). The ferritin molecule is comprised of 24 subunits of two structurally distinct subunit types: H-chain and L-chain. H-ferritin has been shown to regulate immune function, hematopoiesis, hepatocyte apoptosis, and cell differentiation (Recalcati et al. 2008). It has been shown that FHC regulates the intracellular iron which catalyzes the formation of toxic ROS (Cozzi et al. 2000). In this study, we investigated the role of *Cs*FHC as a proinflammatory mediator in activating HSC through the NF-κB signaling pathway. We examined the activation of potential free radical-generating enzymes in LX2 cells treated with *Cs*FHC and investigated the involvement of *Cs*FHC-induced enzyme activation in NF-κB-mediated inflammatory processes. Our results indicate that *Cs*FHC-triggered free radical-mediated NF-κB signaling is an important factor in the chronic inflammation caused by *C. sinensis* infection.

Materials and methods

Reagents

N-acetylcysteine (NAC), allopurinol (ALP; XO inhibitor), diphenyleneiodonium chloride (DPI; NOX inhibitor), and protease inhibitor cocktail were purchased from Sigma-Aldrich (St. Louis, MO, USA). NG-nitro-L-arginine methyl ester (L-NAME; NOS inhibitor) and Bay 11-7082 (IκB-aphosphorylation inhibitor) were purchased from Beyotime Biotechnology (Beyotime Company, Shanghai, China). Polyclonal antibodies against the following proteins were obtained from the indicated sources: NF-κB p65, NF-κB p50, lamin B, calnexin, GAPDH, and horseradish peroxidase (HRP)-conjugated secondary antibodies (Proteintech Company, Chicago, USA); IκB-α, p47phox, p67 Phox, and inducible NOS (iNOS) (Signalway Antibody LLC, Maryland, USA); All other chemicals were purchased from GBCBIO Technologies Inc. (Guangzhou, China).

Cloning, recombinant expression, and purification of $His_{(6)}$-tagged *Cs*FHC

The complete encoding sequence of *Cs*FHC was searched in our draft genome of *C. sinensis* (Wang et al. 2011). The *Cs*FHC full-length cDNA was directly cloned into vector pET-28a(+) (Novagen, USA), using forward primer 5′-GTAGGATCCATGTCCACTTCGTTG-3′ and reverse primer 5′-GCCAAGCTTTTAGTCATCTTCGCC-3′. After DNA sequencing, the recombinant plasmid was transformed into *Escherichia coli* (DE3) (Promega). The expression of recombinant protein was induced with 1 mM isopropyl-L-thio-β-galactopyranoside (IPTG) for 4 h at 37 °C in LB medium containing 50 mg/ml kanamycin. Cell lysate with pET-28a(+)-*Cs*FHC was harvested after centrifugation at 4 °C for 15 min at 8,000×*g* and resuspended in native lysis buffer (50 mM NaH_2PO4, 300 mM NaCl, 5 mM imidazole, pH 8.0), sonicated on ice, and then centrifuged to separate the supernatant and sediment. Recombinant protein was purified by His-bind resin (Novagen) chromatography and dialyzed overnight in phosphate buffered saline (PBS) (pH 7.4). The purified r*Cs*FHC was analyzed by 12 % SDS-PAGE stained with Coomassie brilliant blue G-250. Final recombinant soluble protein concentration was detected by the BCA protein assay kit (Beyotime, Guangzhou, China).

Preparation for antiserum

To prepare anti-*Cs*FHC rat serum, recombinant *Cs*FHC (r*Cs*FHC) was emulsified with complete Freund's adjuvant and subcutaneously immunized with 200 μg of protein for each rat at the first time. Subsequently, each rat was given 100 μg of protein (emulsified with equivalent incomplete Freund's adjuvant) for three booster injections at 2-week intervals. Antiserum was collected at 8 weeks. The antibody titer was determined by enzyme-linked immune sorbent assay (ELISA).

Western blotting analysis

*Cs*ESPs were collected from adult worms according to previously described method (Zheng et al. 2011). Adult worms or metacercariae were crushed and cleaned by centrifugation at 10,000×*g* for 15 min at 4 °C to obtain soluble proteins. The recombinant *Cs*FHC (3 μg/lane), *Cs*ESPs, and the total protein of adult worms and metacercariae (20 μg/lane, respectively) were resolved by 12 % SDS-PAGE and then immobilized onto PVDF membrane. The membranes were blocked with 5 % (*w*/*v*) skim milk at room temperature for 2 h, and then incubated with primary antibody (anti-r*Cs*FHC rat serum, anti-His mouse serum, rat serum infected with *C. sinensis*, and naïve rat serum, respectively, 1:100 dilutions in 0.1 % BSA-PBS) overnight at 4 °C. After washing procedures, the membranes were incubated with HRP-conjugated goat anti-mouse IgG or HRP-conjugated goat anti-rat IgG (1:3,000 dilutions in 0.1 % BSA-PBS, Proteintech Company) for 1 h at RT. The results were detected by ECL method.

RNA extraction and analysis of mRNA expression by quantitative RT-PCR (qRT-PCR)

The extraction of total RNA, complementary DNA synthesis, and PCR amplification were carried out as described elsewhere (Chen et al. 2014; Wang et al. 2011). Briefly, total RNAs from adult worms, excysted metacercariae, metacercariae, and eggs were extracted in Trizol reagent (Invitrogen) according to the manufacturer's instructions. RNA concentrations were detected by nucleic acid/protein analyzer (Beckman Coulter, USA). The preparation of the first-strand cDNA was carried out using RT-PCR kit (TaKaRa, Dalian, China) with the same quantity of total RNA as the template (1 μg). The mRNA expression level of *Cs*FHC at different developmental stages was measured by qRT-PCR, and actin (GenBank accession no. EU109284) was used as the internal control (Wang et al. 2012). The primers were *Cs*FHC: 5′-ATGTCCACTTCGTTGGCT CG-3′ and 5′-CTCGCTCTTCGTCAGACTGCT-3′, respectively, actin: 5′-ACCG TGAGAAGATGACGCAGA-3′ and 5′-GCCAAGTCCAAACGAAGAATT-3′, respectively. Quantitative RT-PCR reactions based on SYBR Green I fluorescence (TaKaRa) were performed by using Bio-Rad CFX96 instrument (Bio-Rad, USA). The PCR amplification program was 95 °C for 30 s, 40 cycles of 95 °C for 5 s, and 60 °C for 20 s. The iQ5 software was used to analyze the relative quantification according to the $2^{-\Delta\Delta CT}$ method (Pfaffl 2001).

Immunolocalization of *Cs*FHC in *C. sinensis* adult worm and metacercaria

Sectioned worms and metacercariae in paraffin wax were deparaffinized and incubated in the rat anti-*Cs*FHC sera (1:200 dilutions). The collected metacercariae were immersed in PBS 0.3 % TritonX-100 for 1 h at RT before being fixed with cold acetone on a glass slide for immunohistochemical analysis. Preimmune rat serum was applied as a negative control. The sections were subsequently incubated with goat anti-rat IgG (1:400 dilutions with 0.1 % BSA in PBS, Alexa Fluor 594, Molecular Probe) for 1 h at RT in the dark, then imaged using a ZEISS Axio Imager Z1 fluorescent microscope.

Iron uptake assay and ferroxidase activity

To remove iron, the recombinant *Cs*FHC protein was incubated for 18 h in a solution of 1 % thioglycolic acid and 0.1 M sodium acetate, pH 5.5. To chelate ferrous irons, excess 2, 2-bipyridine was added to the reaction and the solution was dialyzed exhaustively against 5 mM HEPES, pH 7.0 (Kim et al. 2002). The kinetics of iron uptake were quantified as described previously (Levi et al. 1988) with minor modifications. Briefly, *Cs*FHC proteins or apo-horse ferritin (Sigma) were incubated in 100 mM HEPES (pH 6.0) containing 100 M ferrous ammonium sulfate. The ensuing amber color change was measured at 310 nm at room temperature. The ferro-oxidizing activity of recombinant *Cs*FHC was assayed by employing transferrin as a ferric iron acceptor (Levi et al. 1988). The reaction mixture contained 0.1 M ferrous ammonium sulfate, 4 mg/ml apotransferrin (Sigma), and 0.2 M sodium acetate, pH 7.0, and the recombinant *Cs*FHC at various concentrations. Increase of optical density was recorded at 470 nm for 10 min once the reactions started.

Cell culture and *Cs*FHC treatment

The LX-2 human hepatic stellate cell line was cultured in DMEM (Thermo Hyclone, USA) containing 10 % fetal bovine serum (FBS, NQBB, Australia) and an antibiotic mixture at 37 °C in a humidified 5 % CO_2 humidity. For *Cs*FHC treatment, cells were seeded at ~70 % confluence on 35 or 100 mm culture dishes and grown for 24 h under culture conditions. Cells were gradually deprived of serum by

incubation in 1 % FBS overnight, followed by incubation in serum-free medium for 3 h. These serum-starved cells were treated with 10 nM of *Cs*FHC and incubated for indicated time.

Subcellular fractionation of cell lysates

Cells were homogenized with cold hypotonic lysis buffer (10 mM Tris-HCl, pH 7.4, 250 mM sucrose, 5 mM $MgCl_2$, add fresh protease inhibitor cocktail) on ice for 30 min, centrifuged at 600×*g* for 5 min, and further centrifuged at 13,000×*g* for 20 min. The supernatant was collected and ultracentrifuged at 55,000×*g* for 1.5 h. The resulting supernatant was saved as the cytosol fraction and the pellet was resuspended in lysis buffer (without sucrose) containing 1 % Triton X-100 for isolation of the total membrane fraction. Nuclear proteins were isolated using the nuclear and cytoplasmic extraction kit (Beyotime Biotechnology Inc., Guangzhou, China) according to manufacturer's instructions. The protein concentration of extracts was measured and extracts were stored in aliquots at ~80 °C until use.

Enzymatic activity assays

XO activity was measured using the Amplex Red Xanthine/Xanthine Oxidase Assay Kit (Molecular Probes) according to the manufacturer's instructions as previously described (Ribeiro et al. 2013). NO production was assessed by measuring nitrite/nitrate concentration in culture medium using a Total Nitric Oxide Assay Kit (Beyotime Biotechnology Inc.) according to manufacturer's instructions as previously described (Xiong et al. 2009).

Immunoblot analysis

Total soluble proteins were extracted using RIPA buffer (GBCBIO) and centrifuged at 13,000×*g* for 20 min at 4 °C. The protein concentration in extracts was measured using BCA protein assay kit (Beyotime, China).

Thirty micrograms of total soluble proteins, cytosolic and membranous proteins, or 10 μg of nuclear proteins were separated by SDS-PAGE on 10 % gels, and transferred onto nitrocellulose membranes (Millipore, USA). The membranes were blocked with 5 % skim milk in Tris-buffered saline containing Tween-20 and subsequently probed with antibodies specific for target proteins. After incubating with host-specific secondary antibodies, immune complexes were detected with enhanced chemiluminescence and quantitated by densitometric scanning of the X-ray film with a Image-pro plus 6.0 (Media Cybernetics). Blots were normalized against GAPDH (for cytosolic proteins), calnexin (for membranous proteins) or lamin B (for nuclear proteins).

IL-1β and IL-6 analysis by qRT-PCR

Total RNA was extracted from cells using Trizol reagent and reversely transcribed into cDNA using the reverse transcriptase kit. Equal volumes of single-stranded cDNA product were then used as templates for PCR amplification of the following targets using the indicated primer pairs: IL-1β, 5′-ATGATGGCTTATTACAGTGGCAA-3′ (sense) and 5′-GTCGGAGATTCGTAGCTGGA-3′ (antisense); IL-6, 5′-ACTCACCTCTTCAGAACGAATTG-3′ (sense) and 5′-CCATCTTTGGAAGGTTCAGGTTG-3′ (antisense); and GAPDH (internal control), 5′-GGAGCGAGATCCCTCCAAAAT-3′(sense) and 5′-GGCTGTTGTCATACTTCTCATGG-3′ (antisense). Quantitative real-time PCR based on SYBR Green I fluorescence (TakaRa) was performed as described above. The data were analyzed using the $2^{-\Delta\Delta CT}$ method (Pfaffl 2001).

Cytokine assay

Immunoreactive IL-1β and IL-6 were quantitated in untreated and *Cs*FHC-treated culture supernatant using commercially available ELISA kits (NeoBioscience Technology Inc., China), according to the manufacturer's instructions. A standard curve for each cytokine was generated by known concentration of human recombinant IL-1β or IL-6 protein. The absorbance at 450 nm was then used to calculate the level of IL-1β and IL-6 from the standard curve and adjusted by their dilution factor.

Statistical analysis

Data are expressed as means±S.E.s of three or more independent experiments. Statistical significance was evaluated by one-way ANOVA, followed by a Student's *t* test or Bonferroni's test, as appropriate. Differences in mean values were considered statistically significant at $P<0.05$.

Results

Expression, purification, and identification of r*Cs*FHC

The soluble r*Cs*FHC was expressed with His-tag in *E. coli* BL21 after being induced by 1 mM IPTG at 37 °C for 4 h. The molecular mass of purified protein was about 24 kDa (Fig. 1a), and the final protein concentration was 10 mg/l. Purified r*Cs*FHC could be recognized by rat anti-r*Cs*FHC serum, anti-His tag monoclonal antibody, serum from *C. sinensis*-infected rat and serum from *Cs*ESPs-immunized rat at 24 kDa, while not blotted with serum from naïve rat (Fig. 1b).

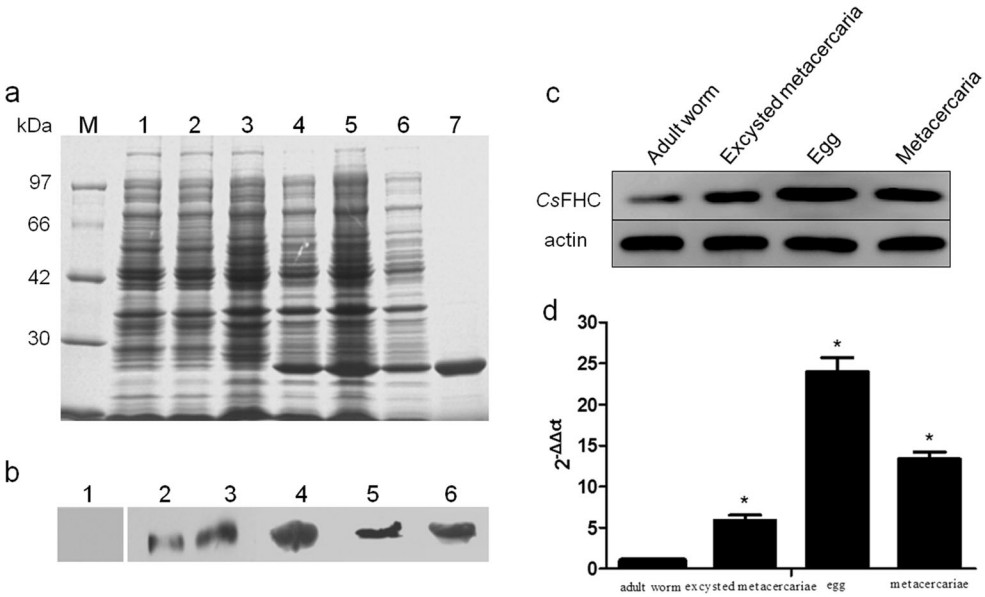

Fig. 1 **a** Expression and purification of r*Cs*FHC by 12 % SDS-PAGE. Protein molecular weight markers (*lane M*), lysate of *E. coli* with pET-28a (+) before induction (*lane 1*) and after induction (*lane 2*), lysate of E. coli with pET28a (+)-*Cs*FHC before induction (*lane 3*) and after induction (*lane 4*), supernatant (*lane 5*), and precipitant (*lane 6*) of lysate of *E. coli* with pET28a (+)-*Cs*FHC after induction (*lane 7*), and the purified recombinant *Cs*FHC protein. **b** Western blotting of r*Cs*FHC. r*Cs*FHC reacted with sera from naive rats (*lane 1*), anti-His tag monoclonal antibody (*lane 2*), sera from *C. sinensis*-infected rats (*lane 3*), sera from rats immunized with the *Cs*ESP (*lane 4*), sera from rats immunized with r*Cs*FHC (*lane 5*). *Cs*ESPs reacted with sera from rats immunized with r*Cs*FHC (*lane 6*). Gene/protein expression analysis of CsFHC at different life cycle stages of C. sinensis. **c** Western blotting analysis. Thirty microgram of total proteins from each life cycle stage were subjected to SDS-PAGE and analyzed. Rat anti-r*Cs*FHC serum was used as primary antibody at a dilution of 1:100. **d** Quantitative real-time PCR analysis. The transcription levels of *Cs*FHC at life stages of adult worm, excysted metacercaria, egg, and metacercaria, and were analyzed by means of the $2^{-\Delta\Delta CT}$ ratio, with *Cs*β-actin serving as the internal standard. *$P<0.05$

Transcriptional level at different developmental stages

The result was calculated according to the previous methods. As shown in Fig. 1c, transcriptional level of *Cs*FHC was detected at the life stages of adult worms, excysted metacercaria, metacercariae, and eggs of *C. sinensis*. The transcription level of *Cs*FHC in egg was about 20 times higher than that in adult worm. The protein level of *Cs*FHC was consistent with the transcriptional level. Egg has the highest expression level of *Cs*FHC protein, followed by adult worm, metacercaria, and excysted metacercaria (Fig. 1d).

Immunohistochemical localization of *Cs*FHC

Figure 2 showed that *Cs*FHC was extensively distributed in metacercariae (Fig. 2e) and in vitellaria and cecum of adult worms (Fig. 2a). No specific fluorescence was detected either in adult worms or in metacercariae when treated with naïve mouse serum (Fig. 2c, g).

Iron incorporation and ferroxidase activity of recombinant *Cs*FHC protein

In preparing the enzymatic assay, purified recombinant *Cs*FHC protein was bleached of incorporated iron to the apo-form. The iron uptake of recombinant *Cs*FHC protein was monitored by measuring optical absorbance of the amber product formed in the presence of ferrous iron and dioxygen. A dose-dependent increase of iron incorporation into recombinant *Cs*FHC was observed (Fig. 3a), and optical absorbance of reaction mixture increased and reached a steady state in about 1 min after the reaction had started. The iron incorporation increased steadily from 1 min after the reaction started until the recombinant *Cs*FHC had been completely saturated. To investigate the ferroxidase activity of recombinant *Cs*FHC protein, the oxidation of ferrous to ferric iron was measured using apotransferrin as an acceptor molecule. The formation of the Fe(III)/transferrin complex was found to increase abruptly during the first 3 min after the reaction started and slowly approached to a steady state by 5 min (Fig. 3b). As was observed in iron incorporation assay, ferroxidase activity was dose-dependent to the amount of recombinant *Cs*FHC added to the reaction mixture. After reaching an oxidation plateau, the second addition of transferrin caused a resumption of the same pattern of ferroxidase activity.

Activation of NOX, XO, and iNOS by *Cs*FHC exposure

We examined whether *Cs*FHC triggered the activation of commonly known free radical-generating enzymes, namely NOX, XO, and NOS, in host cells. Activation of NOX was assessed by determining association of its subunits ($p47^{phox}$

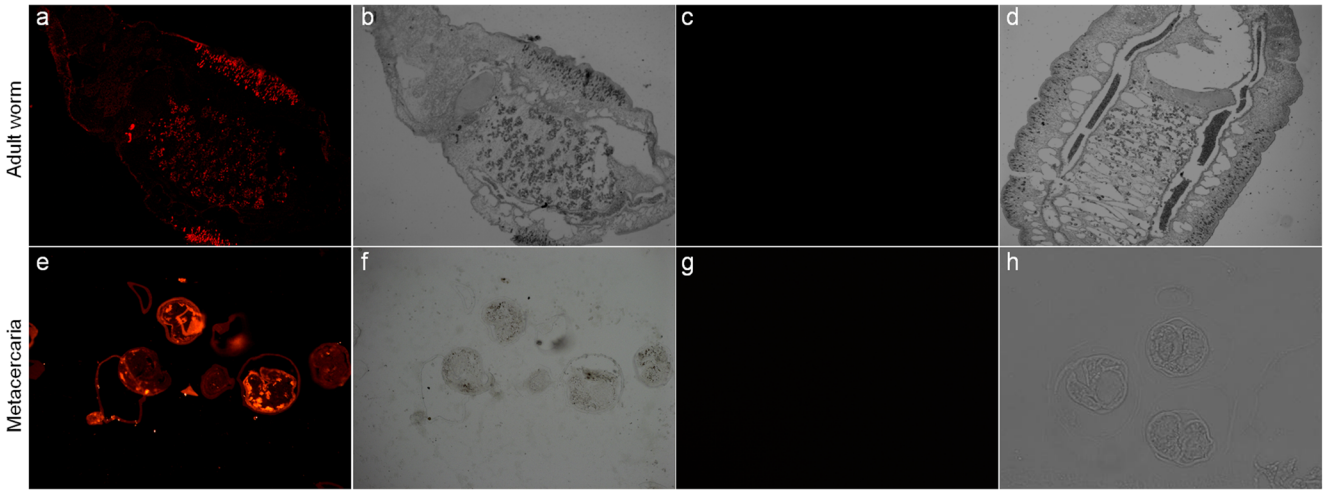

Fig. 2 Immunolocalization of *Cs*FHC in *C. sinensis* metacercariae and adult worms. In adult worms, *Cs*FHC was localized in the vitellaria and cecum (**a**). *Cs*FHC was extensively distributes in metacercariae (**e**). Negative controls were carried out with naïve serum (1:100 *v*/*v*) for adult worms (**g**) and metacercariae (**c**). **b**, **d** Corresponding bright fields for the adult worms. **f**, **h** Corresponding bright fields for metacercariae. The images were magnified at ×100 for adult worms and ×400 for metacercariae, respectively

and p67^{phox}) with the cell membrane. As shown in Fig. 4a, b, increased amounts of immunoreactive p47^{phox} and p67^{phox} were detected in the membrane fraction following a 1-h treatment with *Cs*FHC, with the most significant increases ($P<0.05$) occurring between 9 and 15 h. This result indicates that *Cs*FHC treatment promotes translocation of both p47^{phox} and p67^{phox} from the cytosol to the plasma membrane, suggesting NOX activation. We further investigated the possibility that the increased concentration of nitrite/nitrate reflected the conversion of NO produced by iNOS activation. Immunoblot analyses revealed a clear elevation in iNOS expression as early as 3 h after *Cs*FHC treatment, with the most significant increase occurring at 15 h (Fig. 4d). We also examined the effect of *Cs*FHC on NO generation by measuring nitrite/nitrate concentration in culture media. Nitrite/nitrate formation was significantly increased at 3 h, reaching a peak between 9 and 15 h, followed by a decrease at 24 h ($P<0.05$, Fig. 4e). These time points coincide with the times of increased nitrite/nitrate concentration in culture media. XO activity was significantly increased in cells treated with *Cs*FHC for 3 h, and reached a maximum level at 9 h before gradually declining between 15 and 24 h ($P<0.05$); even at these later time points, XO activity was still higher than that in the untreated control ($P<0.05$, Fig. 4g). These results demonstrate that NOX, XO, and iNOS enzymes in LX2 cells actively participated in the generation of free radicals triggered by *Cs*FHC.

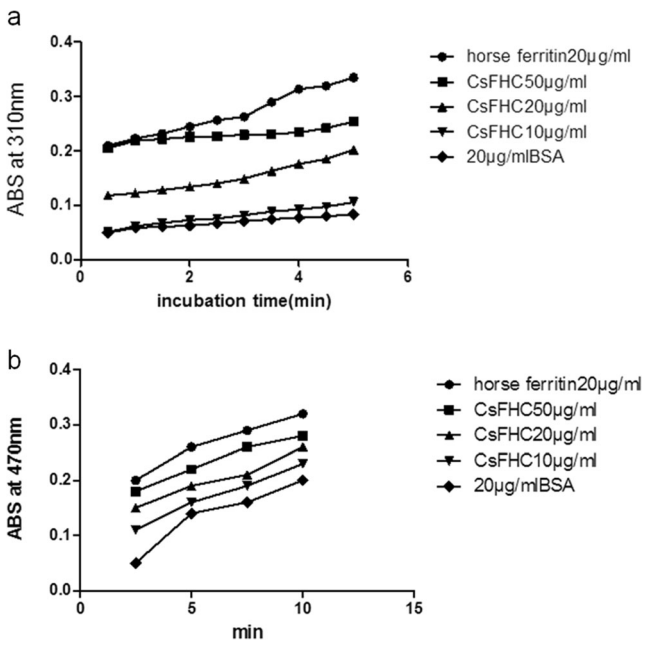

Fig. 3 **a** The iron uptake activity of recombinant *Cs*FHC protein. The reaction mixture contained recombinant *Cs*FHC, 100 μM Fe^{++}, 100 mM HEPES in a volume of 400 μl ($n=3$). **b** Time course of ferroxidase activity of recombinant *Cs*FHC. The formation of the Fe(III)/transferrin complex from ferrous ammonium sulfate and apotransferrin was measured in the presence of recombinant *Cs*FHC. Mean results of triplicate measurements are shown

To confirm that the activation of NOX, XO, and iNOS induced by *Cs*FHC is responsible for free-radical generation, we preincubated cells with a specific inhibitor of each enzyme for 1 h, followed by exposure to *Cs*FHC for 9 h. Pretreatment with DPI, a flavoprotein inhibitor of NOX, significantly inhibited *Cs*FHC-induced accumulation of both p47^{phox} and p67^{phox} in the membrane in a dose-dependent manner ($P<0.05$, Fig. 4a, c). Similarly, pretreatment of cells with ALP (an XO inhibitor) or L-NAME (an NOS inhibitor) resulted in a dose-dependent inhibition of *Cs*FHC-induced XO activation and elevation of nitrite/nitrate concentration

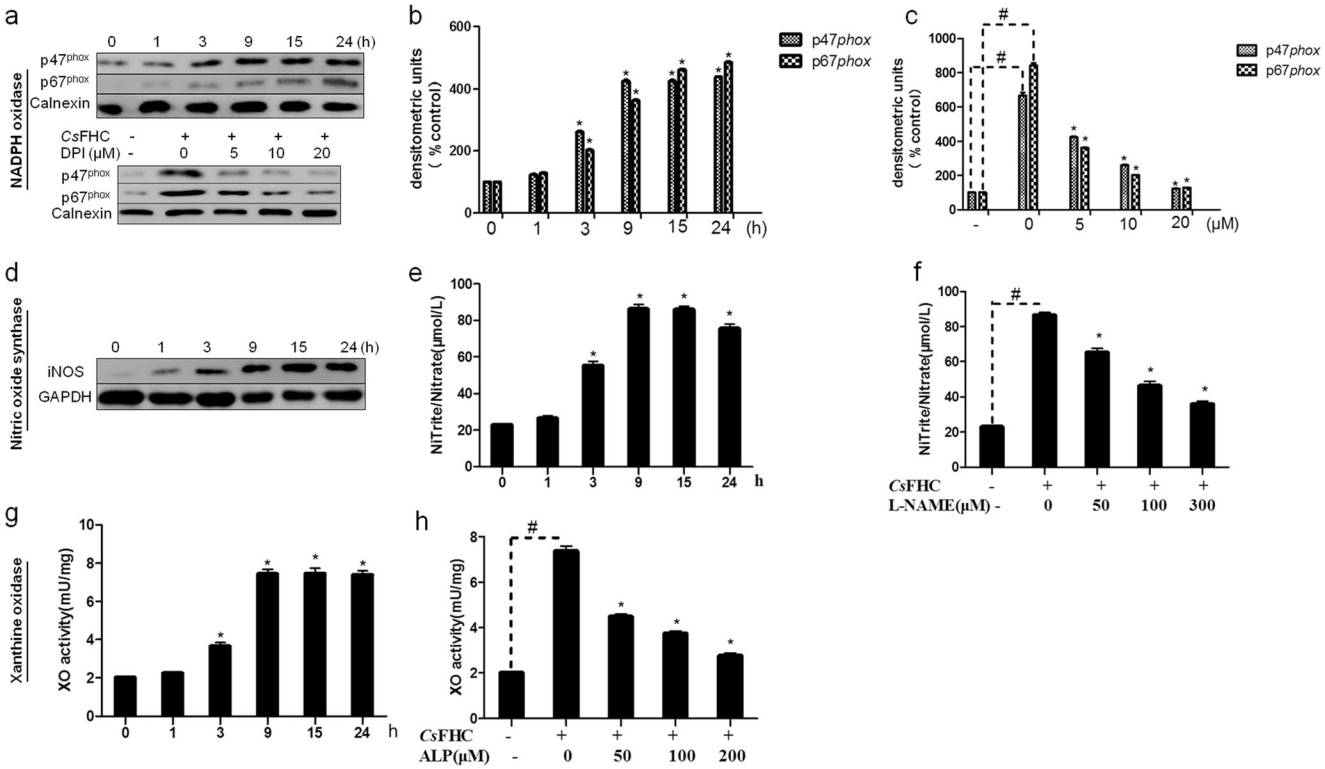

Fig. 4 Effects of *Cs*FHC treatment on the activity of free radical-generating enzymes and inhibition by specific inhibitors. Human hepatic stellate cells were treated with 10 nM of *Cs*FHC for 0–24 h, or cells were preincubated with 5–20 μM of diphenyleneiodonium chloride (**a**), 50–200 μM of allopurinol (**h**), or 50–300 μM of L-NAME (**f**) for 1 h, followed by treatment with 10 nM of ferritin heavy chain for 9 h, and then harvested for immunoblot analysis and enzyme activity assays. **a**, **b**, **c** Accumulation of the NADPH oxidase subunits, $p47^{phox}$ and $p67^{phox}$, in the membrane was assessed by immunoblotting. Calnexin was used as a loading control. Individual data were quantified as densitometric units and normalized with calnexin. Data in the graph are presented as the relative percentage of the untreated control. **d**, **e** Nitric oxide generation in culture media was measured using the Griess reaction after enzymatic conversion of nitrate to nitrite. Total soluble protein (30 μg) was immunoblotted using a polyclonal anti-inducible nitric oxide synthase antibody. GAPDH was used as a loading control. **f** The levels of nitrite/nitrate in culture media were measured in the absence or presence of different concentrations of L-NAME. **g** Xanthine oxidase activity was calculated as mU/mg after normalization to total protein content. **h** The inhibitory effect of allopurinol on excretory/secretory product-induced xanthine oxidase activity. (**b**, **e**, **g**: *$P<0.05$, compared with the zero time point; **c**, **f**, **h**: $^{\#}P<0.05$, compared with excretory/secretory product-untreated control, *$P<0.05$, *Cs*FHC only versus ferritin heavy chain plus each inhibitor)

($P<0.05$, Fig. 4f, h). Taken together, these results suggest that free radicals were generated in *Cs*FHC-treated cells via the activation of NOX, XO, and iNOS.

Induction of NF-κB activation by *Cs*FHC treatment

It has been reported that the activation of NF-κB can be controlled by ROS produced in response to various stimuli (Gloire et al. 2006). Moreover, increased levels of NF-κB and iNOS have been shown to colocalize in the bile duct epithelium of hamsters infected by *O. viverrini*, leading to oxidative DNA damage and elevated inflammatory cell infiltration (Pinlaor et al. 2006). These findings prompted us to examine whether *Cs*FHC exposure was associated with NF-κB activation. The cytosolic and nuclear fractions of cells treated with 10 nM of *Cs*FHC for 0–24 h were used to determine the degradation of IκBα and nuclear translocation of the NF-κB subunits, p65 and p50, by immunoblot analysis. As shown in Fig. 5a, b, cytosolic IκBα protein was almost completely degraded at 9 h, concomitant with the time-dependent nuclear accumulation of NF-κB p50 and p65 subunits (Fig. 5d, e). These results demonstrate that *Cs*FHC treatment led to NF-κB activation in LX2 cells.

Involvement of *Cs*FHC-triggered free radicals in NF-κB activation

To assess the role of intracellular free radicals generated in response to *Cs*FHC exposure in NF-κB activation, we preincubated LX2 cells with the antioxidant NAC (1–10 mM) for 1 h before adding 10 nM of *Cs*FHC, and then collected cytosolic and nuclear fractions after 9 h for immunoblot analysis. *Cs*FHC-mediated IκBα degradation in the cytosol was significantly inhibited in a dose-dependent manner by NAC, with 10 mM of NAC reducing degradation by ~50 % ($P<0.05$, Fig. 5a, c). Nuclear translocation of NF-κB p50 and p65 subunits was also suppressed to levels below those in *Cs*FHC-treated controls (~260 % inhibition) by 5 mM of NAC

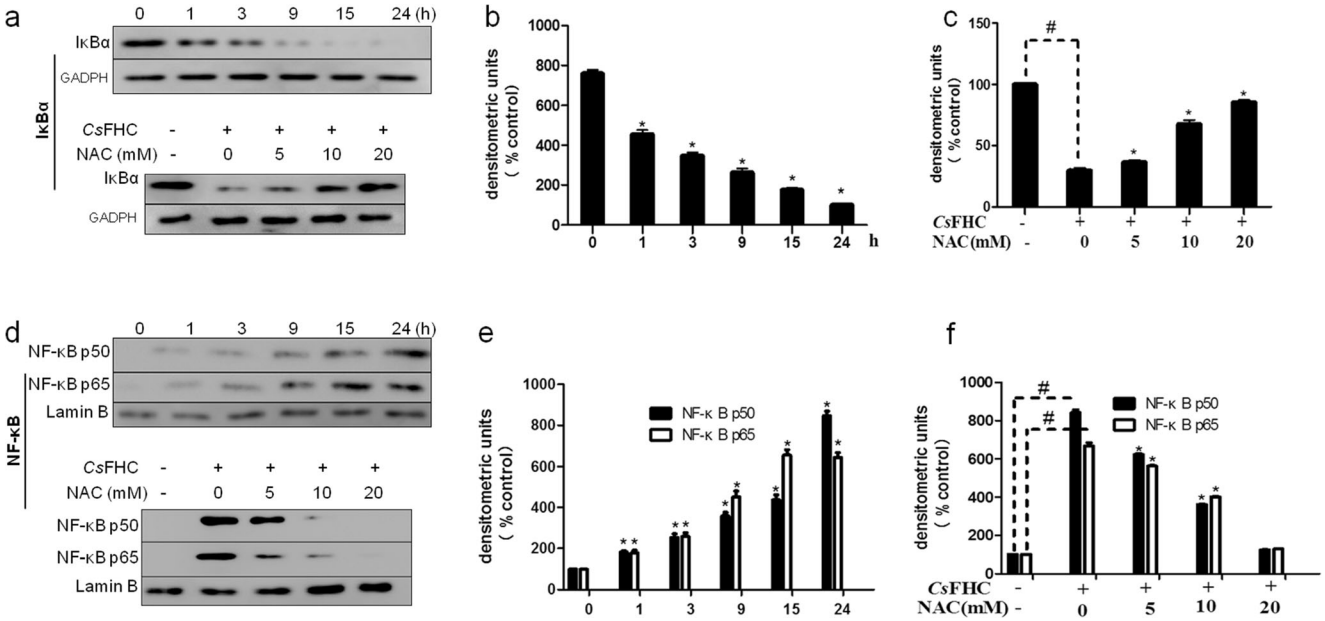

Fig. 5 *Cs*FHC-induced NF-κB activation and inhibitory effect of *N*-acetylcysteine. After treatment with 10 nM of *Cs*FHC for the indicated times or cells were preincubated with different concentrations of *N*-acetylcysteine for 1 h before incubating with 10 nM of *Cs*FHC for 9 h, degradation of cytosolic IκBα and nuclear accumulation of the NF-κB subunits, p50 and p65, were determined by immunoblotting using polyclonal antibodies against IκBα (**a**), p50 and p65 (**d**). Protein bands were quantified and the densities of IκB-α and p50/p65 bands were normalized to those of GAPDH and lamin B bands, respectively. The normalized IκB-α, p50 and p65 band densities from each group are presented as a percentage of those in ferritin heavy chain-untreated controls. Values are means±S.E.s of three independent experiments ($^{\#}P<0.05$, compared with ferritin heavy chain-untreated controls; **c**: $^{*}P<0.05$, compared with excretory/secretory product-untreated control; **f** $^{*}P<0.05$, *Cs*FHC only versus *Cs*FHC plus different concentrations of *N*-acetylcysteine)

($P<0.05$, Fig. 5d, f), demonstrating that NAC attenuated *Cs*FHC-induced NF-κB activation by scavenging free radicals triggered by *Cs*FHC. Because free radicals were produced by the activation of NOX, XO, and iNOS in *Cs*FHC-treated cells, we explored the effects of each enzyme inhibitor on NF-κB activation. Preincubation of LX2 cells with 10 μM of DPI, 100 μM of ALP or 100 μM of L-NAME for 1 h prior to *Cs*FHC treatment reduced IκBα degradation in the cytosol by ~67, ~24, and ~40 %, respectively, relative to that induced by *Cs*FHC alone ($P<0.05$, Fig. 6a, b). The relative effectiveness of these inhibitors suggests that ROS generated by NOX activity are the most effective inducers of NF-κB activation. Concomitant with this, the administration of inhibitors resulted in a significant disruption of *Cs*FHC-induced NF-κB p50 and p65 nuclear accumulation ($P<0.05$, Fig. 6c, d), indicating that the activities of these enzymes are closely associated with NF-κB activation.

Proinflammatory cytokines IL-1β and IL-6 increased by *Cs*FHC-induced NF-κB activation

It is generally accepted that helminth infection contributes to inflammatory responses in host cells. In particular, animal models of *O. viverrini* infection have shown accumulation of liver fluke-associated antigens in the intra- and extrahepatic bile duct epithelium, accompanied by marked local inflammatory responses (Vennervald and Polman 2009). Therefore, we analyzed the mRNA expression patterns of the most common proinflammatory cytokines, IL-1β and IL-6, during a 1–24 h *Cs*FHC exposure. Quantitative real-time PCR analyses revealed a significant elevation in the expression of cytokines with 1 h of *Cs*FHC exposure ($P<0.05$). IL-1β expression reached a maximal level at 9 h, then declined afterwards, whereas IL-6 expression gradually increased up to 24 h ($P<0.05$, Fig. 7a). Because NF-κB is a key transcription factor involved in initiating the inflammatory cascade and regulating inflammatory mediators, we investigated whether NF-κB inactivation attenuated *Cs*FHC-induced upregulation of IL-1β and IL-6 mRNA expression. Cells were preincubated with different concentrations of the NF-κB inhibitor, Bay11-7082, for 1 h before treatment with 10 nM of *Cs*FHC for 9 h. As shown in Fig. 7b, this irreversible inhibitor suppressed the *Cs*FHC-induced increase in both IL-1β and IL-6 mRNA in a dose-dependent manner ($P<0.05$), suggesting that NF-κB signaling pathways are involved in the inflammatory responses of LX2 cells during *Cs*FHC exposure. To validate the correlation of mRNA expression with protein level, we measured the level of each cytokine in the culture supernatants of 9 h *Cs*FHC-treated cells, as accessed by ELISA. The levels of both IL-1β and IL-6 secretion were significantly increased ($P<0.05$), compared with that of the control (Figs. 7c, d). Taken together,

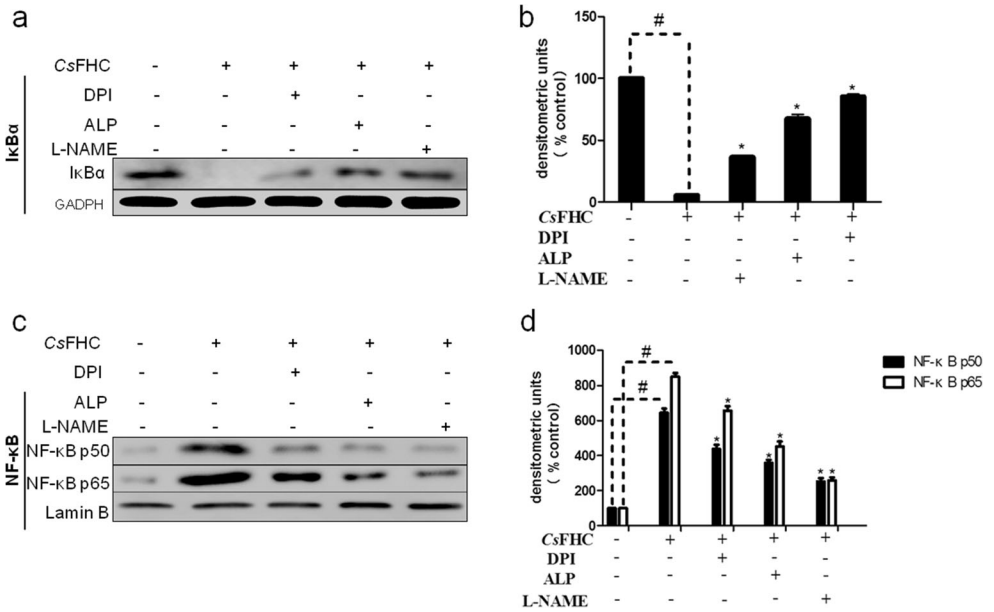

Fig. 6 NF-κB inactivation by NADPH oxidase, xanthine oxidase, and nitric oxide synthase inhibitors in *Cs*FHC-treated cells. Cells were preincubated with 10 μM of DPI, 100 μM of ALP, or 100 μM of L-NAME for 1 h, followed by treatment with 10 nM of *Cs*FHC for 9 h. Cytosolic and nuclear proteins were subjected to immunoblot analysis for IκB-α, NF-κB p50 and p65 expression levels. **a** Representative immunoblot of IκB-α expression. **b** Representative immunoblot of NF-κB p50 and p65 expression. Individual data were quantified and normalized to GAPDH (IκB-α) or lamin B (p50 and p65). Values in graphs are presented as a percentage of those in untreated controls, expressed as means±S.E.s of three independent experiments ($^{\#}P<0.05$, compared with *Cs*FHC-untreated controls; $^{*}P<0.05$, *Cs*FHC only versus *Cs*FHC plus different concentrations of *N*-acetylcysteine)

these results indicated that the expressions of IL-1β and IL-6 were transcriptionally and translationally upregulated by *Cs*FHC.

Discussion

A major pathological consequence of liver fluke infection is inflammation of the hepatobiliary system of both naturally infected humans and experimentally infected animals (Lim et al. 2008; Rim 2005; Vennervald and Polman 2009; Yoon et al. 2001). In the present study, we identified and characterized a ferritin heavy chain protein of *C. sinensis*. We obtained soluble and stable r*Cs*FHC, which could be recognized by both serum from *C. sinensis*-infected and serum from *C. sinensis* ESP-immunized mouse. qRT-PCR analysis demonstrated that *Cs*FHC can be detected in different developmental stages of *C. sinensis* including adult worm, metacercaria, and egg stages, indicating that *Cs*FHC was expressed across all stages of *C. sinensis* (Fig. 1). In this study, LX-2 cell line which retains features of HSCs was used as a model of HSC-induced liver fibrosis in vitro (Xu et al. 2005). We provided evidence that, LX2 cells exposed to *C. sinensis* *Cs*FHC generate free radicals by the activation of NF-κB through NOX, XO, and iNOS, and proinflammatory molecules, IL-1β and IL-6, were subsequently upregulated. These results demonstrate that free radicals function as key triggering modulators of host NF-κB-mediated inflammation in response to *Cs*FHC.

In hepatic fibrosis, HSCs become activated and transdifferentiate into proliferative myofibroblast cells upon chronic exposure to inflammatory environment (Friedman 2008). HSCs are the central cell type in the liver's fibrogenic process and activated in many conditions that lead to liver fibrosis (Friedman 2004). Free radicals actively participate in diverse physiological processes, including cell growth, survival, induction and maintenance of the transformed state, cellular senescence, apoptosis, and even necrosis (Nam et al. 2012). We examined NF-κB activation in LX2 cells treated with *C. sinensis* *Cs*FHC. Our results revealed that *Cs*FHC promoted the degradation of cytosolic IκB-α, indicated by gradual increase in nuclear translocation of NF-κB p50 and p65 subunits. These inhibitory effects on enzyme activation were correlated with a reduction in the levels of intracellular ROS and NO, indicating the role of enzymatic free-radical generation in the response to *Cs*FHC (Fig. 4).

*Cs*FHC-induced activation of NF-κB was dose-dependently attenuated by the ROS scavenger, NAC (Fig. 5). Furthermore, pretreatment of cells with DPI, ALP, or L-NAME substantially antagonized *Cs*FHC-induced activation of NF-κB (Fig. 6), demonstrating that free radicals generated by the activation of *Cs*FHC played important roles in the activation of the NF-κB pathway. A number of studies

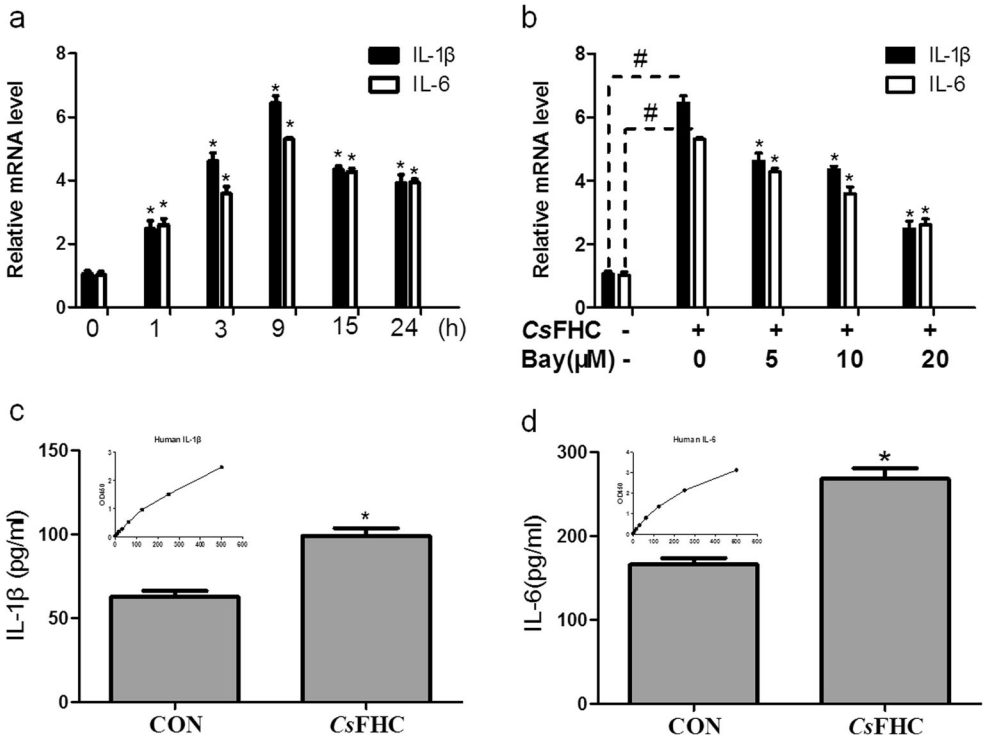

Fig. 7 Expression of IL-1β and IL-6 in *Cs*FHC-treated cells. **a** Cells were treated with 10 nM of *Cs*FHC, harvested after 0 to 24 h, and subjected to Quantitative real-time PCR analysis. **b** Cells were preincubated with 5–20 μM of Bay11-7082 for 1 h, followed by treatment with 10 nm of ferritin heavy chain for 9 h. IL-1β and IL-6 mRNAs were detected by the reverse transcription-PCR. Each band was quantified and normalized to GAPDH band density. The ratios of IL-1β and IL-6 mRNAs to GAPDH from each group are presented as a percentage of that at zero time (**a**) or in ferritin heavy chain-untreated controls (**b**). **c**, **d** Cells were incubated with 10 nM of *Cs*FHC or an equal volume of PBS (control; *CON*) for 9 h, and the production of IL-1β or IL-6 in culture supernatants was determined by ELISA. Data are presented as means±S.E.s of three independent experiments. **P*<0.05 compared with the control. Values are means±S.E.s of three independent experiments (**P*<0.05, compared with zero time (**a**) or ferritin heavy chain only versus ferritin heavy chain plus Bay11-7082 (Bay) (**b**); #*P*<0.05, compared with ferritin heavy chain-untreated controls)

also suggested that the redox status of cells participates in modulating NF-κB activation (Asehnoune et al. 2004; Gloire et al. 2006; Kim et al. 2008; Pantano et al. 2006). Consistent with our results, enzymatic free-radical generation has been reported in liver fluke-infected animals. For instance, ROS-induced apoptosis in rat eosinophils treated with *F. hepatica* ESPs is attenuated in the presence of DPI (Serradell et al. 2009). Finally, our experiments showed that *Cs*FHC-induced NF-κB activation was associated with an increase in the levels of IL-1β and IL-6 mRNA and proteins (Fig. 7). IL-1β and IL-6 are pleiotropic cytokines that have diverse potentiating effects on proliferation, differentiation, and apoptosis, as well as on local and systemic inflammatory responses (Nam et al. 2012; Naugler and Karin 2008). IL-1β can cause inflammation and induce the expression of proinflammatory genes. In addition, IL-1β promotes the generation of ROS (Brigelius-Flohe et al. 2004). Our results suggested that proinflammatory cytokine production in host cells stimulated by *Cs*FHC serves as a link to immune responses.

In conclusion, we have identified a new gene *Cs*FHC from *C. sinensis* and investigated the role of *Cs*FHC to trigger free radicals and mediate NF-κB inflammation signaling in human hepatic stellate cells LX2. We demonstrated that *Cs*FHC was a component of *Cs*ESPs. The present study provides insight into the biochemical mechanism by which *C. sinensis Cs*FHC induce inflammatory responses in host cells. Given the direct relationship between chronic inflammation and cancers, our findings implied that free radicals may play pivotal roles in the pathology that occurs in the liver tissues system during *C. sinensis* infection, and free radicals may contribute to the severe inflammation in clonorchiasis that has been associated with hepatic fibrosis. Further investigations on upstream and downstream elements in the NF-κB signaling pathway are required to elucidate the mechanisms underlying the progression of clonorchiasis.

Acknowledgments This work was supported by the National Key Basic Research and Development Project of China (973 project; no. 2010CB530000), National S & T Major Program (no. 2012ZX10004-220), National Natural Science Foundation of China (no. 81101270 and no. 81171602), Fundamental Research Funds for the Central Universities (no. 3164015).

References

Asehnoune K, Strassheim D, Mitra S, Kim JY, Abraham E (2004) Involvement of reactive oxygen species in Toll-like receptor 4-dependent activation of NF-kappa B. J Immunol 172:2522–2529

Brigelius-Flohe R, Banning A, Kny M, Bol GF (2004) Redox events in interleukin-1 signaling. Arch Biochem Biophys 423:66–73

Chen T, Ning D, Sun H, Li R, Shang M, Li X, Wang X, Chen W, Liang C, Li W, Mao Q, Li Y, Deng C, Wang L, Wu Z, Huang Y, Xu J, Yu X (2014) Sequence analysis and molecular characterization of *Clonorchis sinensis* hexokinase, an unusual trimeric 50-kDa glucose-6-phosphate-sensitive allosteric enzyme. PLoS One 9:e107940

Cozzi A, Corsi B, Levi S, Santambrogio P, Albertini A, Arosio P (2000) Overexpression of wild type and mutated human ferritin H-chain in HeLa cells: in vivo role of ferritin ferroxidase activity. J Biol Chem 275:25122–25129

Elsharkawy AM, Mann DA (2007) Nuclear factor-kappaB and the hepatic inflammation-fibrosis-cancer axis. Hepatology 46:590–597

Friedman SL (2004) Mechanisms of disease: mechanisms of hepatic fibrosis and therapeutic implications. Nat Clin Pract Gastroenterol Hepatol 1:98–105

Friedman SL (2008) Mechanisms of hepatic fibrogenesis. Gastroenterology 134:1655–1669

Gloire G, Legrand-Poels S, Piette J (2006) NF-kappaB activation by reactive oxygen species: fifteen years later. Biochem Pharmacol 72:1493–1505

Hu F, Hu X, Ma C, Zhao J, Xu J, Yu X (2009) Molecular characterization of a novel *Clonorchis sinensis* secretory phospholipase A(2) and investigation of its potential contribution to hepatic fibrosis. Mol Biochem Parasitol 167:127–134

Huang Y, Li W, Huang L, Hu Y, Chen W, Wang X, Sun J, Liang C, Wu Z, Li X, Xu J, Yu X (2012) Identification and characterization of myophilin-like protein: a life stage and tissue-specific antigen of *Clonorchis sinensis*. Parasitol Res 111:1143–1150

Kim TY, Joo IJ, Kang SY, Cho SY, Hong SJ (2002) *Paragonimus westermani*: molecular cloning, expression, and characterization of a recombinant yolk ferritin. Exp Parasitol 102:194–200

Kim YJ, Choi MH, Hong ST, Bae YM (2008) Proliferative effects of excretory/secretory products from *Clonorchis sinensis* on the human epithelial cell line HEK293 via regulation of the transcription factor E2F1. Parasitol Res 102:411–417

Kim TI, Na BK, Hong SJ (2009) Functional genes and proteins of *Clonorchis sinensis*. Korean J Parasitol 47(Suppl):S59–S68

Levi S, Luzzago A, Cesareni G, Cozzi A, Franceschinelli F, Albertini A, Arosio P (1988) Mechanism of ferritin iron uptake: activity of the H-chain and deletion mapping of the ferro-oxidase site. A study of iron uptake and ferro-oxidase activity of human liver, recombinant H-chain ferritins, and of two H-chain deletion mutants. J Biol Chem 263:18086–18092

Liang P, Zhang F, Chen W, Hu X, Huang Y, Li S, Ren M, He L, Li R, Li X, Xu J, Wu Z, Lu G, Yu X (2013) Identification and biochemical characterization of adenylate kinase 1 from *Clonorchis sinensis*. Parasitol Res 112:1719–1727

Lim JH, Mairiang E, Ahn GH (2008) Biliary parasitic diseases including clonorchiasis, opisthorchiasis and fascioliasis. Abdom Imaging 33: 157–165

Lv X, Chen W, Wang X, Li X, Sun J, Deng C, Men J, Tian Y, Zhou C, Lei H, Liang C, Yu X (2012) Molecular characterization and expression of a cysteine protease from *Clonorchis sinensis* and its application for serodiagnosis of clonorchiasis. Parasitol Res 110:2211–2219

Ma C, Hu X, Hu F, Li Y, Chen X, Zhou Z, Lu F, Xu J, Wu Z, Yu X (2007) Molecular characterization and serodiagnosis analysis of a novel lysophospholipase from *Clonorchis sinensis*. Parasitol Res 101: 419–425

Morgan MJ, Liu ZG (2011) Crosstalk of reactive oxygen species and NF-kappaB signaling. Cell Res 21:103–115

Nam JH, Moon JH, Kim IK, Lee MR, Hong SJ, Ahn JH, Chung JW, Pak JH (2012) Free radicals enzymatically triggered by *Clonorchis sinensis* excretory-secretory products cause NF-kappaB-mediated inflammation in human cholangiocarcinoma cells. Int J Parasitol 42:103–113

Naugler WE, Karin M (2008) The wolf in sheep's clothing: the role of interleukin-6 in immunity, inflammation and cancer. Trends Mol Med 14:109–119

Pantano C, Reynaert NL, van der Vliet A, Janssen-Heininger YM (2006) Redox-sensitive kinases of the nuclear factor-kappaB signaling pathway. Antioxid Redox Signal 8:1791–1806

Pfaffl MW (2001) A new mathematical model for relative quantification in real-time RT-PCR. Nucleic Acids Res 29:e45

Pinlaor S, Tada-Oikawa S, Hiraku Y, Pinlaor P, Ma N, Sithithaworn P, Kawanishi S (2005) *Opisthorchis viverrini* antigen induces the expression of Toll-like receptor 2 in macrophage RAW cell line. Int J Parasitol 35:591–596

Pinlaor S, Hiraku Y, Yongvanit P, Tada-Oikawa S, Ma N, Pinlaor P, Sithithaworn P, Sripa B, Murata M, Oikawa S, Kawanishi S (2006) iNOS-dependent DNA damage via NF-kappaB expression in hamsters infected with *Opisthorchis viverrini* and its suppression by the antihelminthic drug praziquantel. Int J Cancer 119:1067–1072

Recalcati S, Invernizzi P, Arosio P, Cairo G (2008) New functions for an iron storage protein: the role of ferritin in immunity and autoimmunity. J Autoimmun 30:84–89

Ribeiro M, Silva AC, Rodrigues J, Naia L, Rego AC (2013) Oxidizing effects of exogenous stressors in Huntington's disease knock-in striatal cells—protective effect of cystamine and creatine. Toxicol Sci 136:487–499

Rim HJ (2005) Clonorchiasis: an update. J Helminthol 79:269–281

Serradell MC, Guasconi L, Cervi L, Chiapello LS, Masih DT (2007) Excretory-secretory products from *Fasciola hepatica* induce eosinophil apoptosis by a caspase-dependent mechanism. Vet Immunol Immunopathol 117:197–208

Serradell MC, Guasconi L, Masih DT (2009) Involvement of a mitochondrial pathway and key role of hydrogen peroxide during eosinophil apoptosis induced by excretory-secretory products from *Fasciola hepatica*. Mol Biochem Parasitol 163:95–106

Theil EC (1987) Ferritin: structure, gene regulation, and cellular function in animals, plants, and microorganisms. Annu Rev Biochem 56: 289–315

Vennervald BJ, Polman K (2009) Helminths and malignancy. Parasite Immunol 31:686–696

Wang X, Chen W, Huang Y, Sun J, Men J, Liu H, Luo F, Guo L, Lv X, Deng C, Zhou C, Fan Y, Li X, Huang L, Hu Y, Liang C, Hu X, Xu J, Yu X (2011) The draft genome of the carcinogenic human liver fluke *Clonorchis sinensis*. Genome Biol 12(10):R107

Wang X, Chen W, Lv X, Tian Y, Men J, Zhang X, Lei H, Zhou C, Lu F, Liang C, Hu X, Xu J, Wu Z, Li X, Yu X (2012) Identification and characterization of paramyosin from cyst wall of metacercariae implicated protective efficacy against *Clonorchis sinensis* infection. PLoS One 7:e33703

Xiong J, Lu H, Lu K, Duan Y, An L, Zhu C (2009) Cadmium decreases crown root number by decreasing endogenous nitric oxide, which is indispensable for crown root primordia initiation in rice seedlings. Planta 230:599–610

Xu L, Hui AY, Albanis E, Arthur MJ, O'Byrne SM, Blaner WS, Mukherjee P, Friedman SL, Eng FJ (2005) Human hepatic stellate cell lines, LX-1 and LX-2: new tools for analysis of hepatic fibrosis. Gut 54:142–151

Yoon BI, Choi YK, Kim DY, Hyun BH, Joo KH, Rim HJ, Lee JH (2001) Infectivity and pathological changes in murine clonorchiasis:

comparison in immunocompetent and immunodeficient mice. J Vet Med Sci 63:421–425

Zheng M, Hu K, Liu W, Hu X, Hu F, Huang L, Wang P, Hu Y, Huang Y, Li W, Liang C, Yin X, He Q, Yu X (2011) Proteomic analysis of excretory secretory products from *Clonorchis sinensis* adult worms: molecular characterization and serological reactivity of a excretory-secretory antigen-fructose-1,6-bisphosphatase. Parasitol Res 109: 737–744